

MOTION CONTRAST IMAGING USING ZEBRAFISH

To observe the earliest point of the transition between dry AMD and wet AMD, the choroidal neovascularization must be visualized before it tries to break through Bruch's membrane. Using the motion contrast methods of optical coherence tomography, the vascular visualization capabilities must be determined in order to apply it as a screening tool for eye care. For the first proof-of-concept experiments, an animal model of vasculature is used. By using a non-retinal vascular model in a microscopy setup, the expected bulk motion effects during imaging will be reduced compared to a retinal imaging system.

4.1 Choosing Zebrafish as the Animal Model

There are several requirements of an optimal animal model for SDOCT imaging, including but not limited to:

- Transparency allows for direct optical access to all of the layers within the animal
- Feature sizes approximately the same size as the resolution of the system
- Thickness of animal is less than the imaging depth of the SDOCT system
- A well established model of vasculature of the animal allows for direct comparison of measured motion contrast to expected

Zebrafish (*Danio rerio*) is an excellent animal model of vasculature. With the addition of the chemical phenylthiourea (PTU) applied to zebrafish embryos at time points earlier than 1 dpf (days post fertilization), the pigment production in the animal is inhibited. Without the production of the highly absorptive pigment, the zebrafish can grow for several days transparently, making it ideal for optical imaging. The ideal age to image the zebrafish is around 3-4 dpf, where the features have grown large enough to be visualized with an OCT

system but the entire animal thickness is small enough to be imaged using SDOCT. Around 5 dpf with the pigment blocker applied, the zebrafish begin to develop pigment, limiting the imaging regions of the sample.

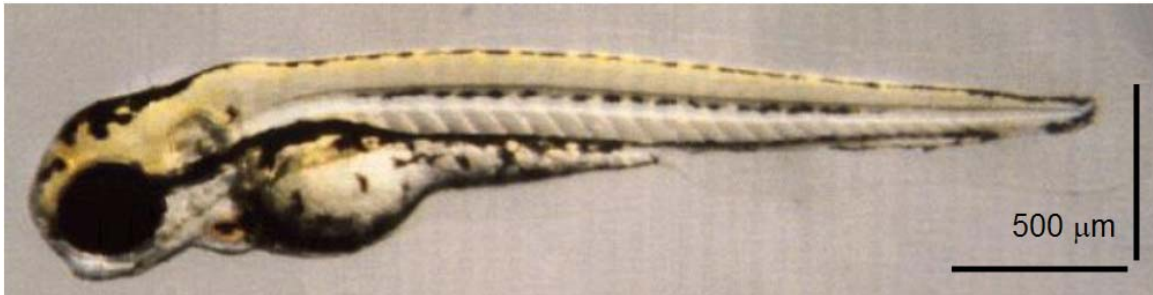


Figure 4.1: Bright field illumination confocal image of 3 dpf zebrafish without the addition of the pigment blocker. Approximate scale bars were added to the image reproduced from [1].

Variant strains of zebrafish have been developed which contain green fluorescent protein (GFP) labeled vasculature. This has provided valuable insight into the vascular formation of the zebrafish during development for the ability to confocally image the vasculature for these zebrafish strains. These images can also be created by injecting a fluorescent dye and imaging the fluorescence confocally. With the availability of facilities allowing for the acquisition of zebrafish embryos and the short required development time for samples, the zebrafish is an ideal animal model for SDOCT motion contrast imaging.

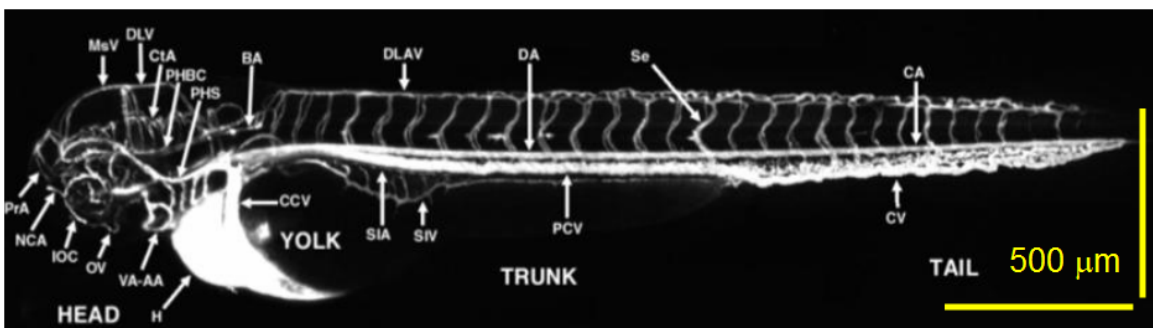


Figure 4.2: Confocal fluorescence image of 3 dpf zebrafish with fluorescent dye injected within its vasculature. Approximate scale was added to image reproduced from [2].

4.2 Creating SDOCT Images

To image the zebrafish in the SDOCT, the system must be set up for microscopy. With an expected axial resolution in tissue of approximately $6\ \mu\text{m}$ due to the light source properties, the transverse resolution was chosen to try and match this resolution. In SDOCT all of the depths are measured at the same time, each with its own transverse resolution. For a transverse resolution of approximately $5\ \mu\text{m}$ at the focus, the resolution decreases at depths away from the focus, increasing to $7\ \mu\text{m}$ over a depth range of $50\ \mu\text{m}$. The polarization controllers (PC) applied to each of the arms of the interferometer are used to adjust the polarization of the light traveling through the fiber coupler to maximize the interference fringe signals measured at the spectrometer.

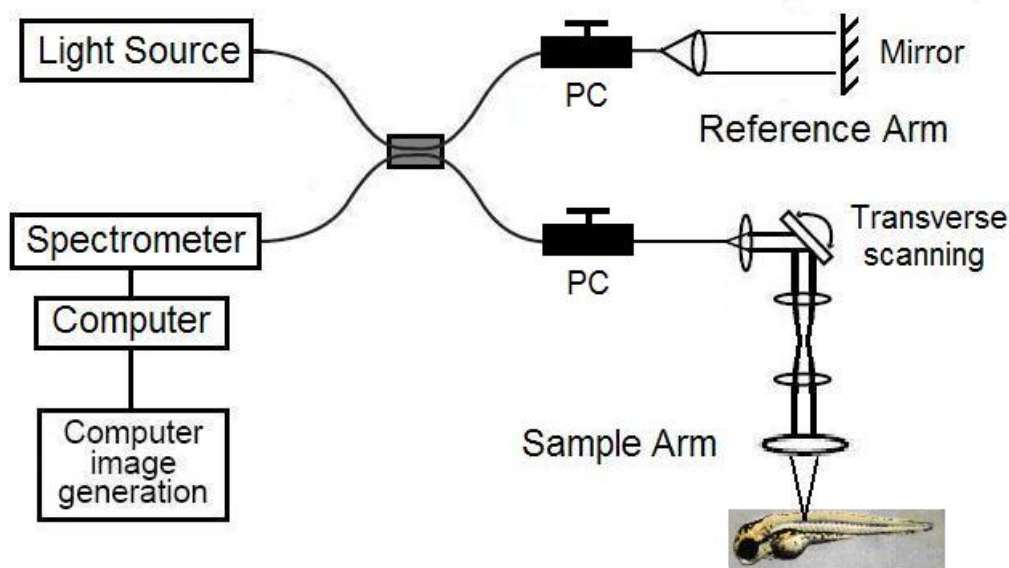


Figure 4.3: Schematic of the experimental fiber optic SDOCT microscopy system. PC: polarization controller.

Creating OCT images from the spectrometer data requires several processing steps before the Fourier transform is performed, with the most important being the linearization of the data to k -space. The spectrometer samples the interferometric signal in k -space, but in general the spacing between neighbouring CCD pixels is not uniform across the entire

measurement. The spectrometer data must be linearized in k-space to allow for a proper Fourier transform to be calculated.

To calculate an A-scan from the spectrometer measurements, it is also important to remove the source spectral component before computing the Fourier transform. Without removing the spectral component from the reference arm, the A-scan calculated as the magnitude of the Fourier transform appears in the form:

$$|FT(P(k))|^2 \propto P_R^2 |\tilde{f}_C(z)|^2 + \sum_j P_R P_{Sj} |\tilde{f}_C(z - z_j)|^2. \quad (4.1)$$

In this case the OCT coherence function $|\tilde{f}_C(z)|^2$, defined in Chapter 2.2 as determined by the shape of the light source spectra, sets a lot of the image properties. In general, for OCT imaging the power from the reference arm dominates over all of the sample reflections such that $P_R \gg P_{Sj}$. For this assumption the DC component of the image is substantial, causing the side lobes of the coherence function for this term to interfere with the rest of the image. As discussed in Chapter 2.8, the removal of the source spectra before the Fourier transform is expected to remove the DC component of the OCT image:

$$|\tilde{I}(z)|^2 = |FT(P(k) - P_R(k))|^2 \propto \sum_j P_R P_{Sj} |\tilde{f}_C(z - z_j)|^2. \quad (4.2)$$

There are several methods to determine the source spectra without the interference signal associated with a spectrometer measurement in SDOCT. By simply blocking the sample arm, the reference arm spectra can be measured directly. While this method is adequate for many methods, when the measured spectrum shape or intensity changes due to fluctuations or image re-alignment, artifacts appear in the B-scan based on the discrepancy between the measured and removed source spectra.

To reduce any of the fluctuation effects of the measured reference spectrum, the background spectra should be measured or calculated from data taken at the same time as

the SDOCT imaging. While mechanically diverting or blocking the sample arm during a buffered acquisition of the spectrometer data is possible, it is not ideal in many cases. There is a very simple method of calculating the background spectra using all of the data acquired during a single B-scan. The assumption is that all of the interference fringes within an image are of comparable intensity with a random distribution of depths such that averaging the fringes will all cancel each other out. For N_X A-scans used to create a B-scan, averaging all of the spectrometer measurements for this B-scan will create the background average spectra to use for A-scan calculation [3]:

$$\bar{P}(k) = \frac{1}{N_X} \sum_j P_j(k). \quad (4.3)$$

In certain imaging cases, the assumption used for determining the background spectra does not hold. One example is when the sample contains specular reflections, which are highly localized reflections which are much stronger than the rest of the sample reflections. Averaging the fringes in this case cannot completely cancel out these large reflections, causing the remaining portion of the fringe to appear across the entire B-scan when the averaged spectra is used in the calculation of each A-scan. A weighted average of the interference spectra makes it possible to minimize the effect of the scans which contain specular reflections.

For spectrometer measurement j which contains a maximum reflectance of $R_{j,Max}$ located at a depth position $z_{j,Max}$, the removal of the averaged spectra results in approximately the maximum interference reflection:

$$(P_j(k) - \bar{P}(k))^2 \propto R_{j,Max} \cos^2(kz_{j,Max}). \quad (4.4)$$

This fact results in the weighted background spectrum calculation of:

$$P_R(k) = \frac{\sum_j w_j P_j(k)}{\sum_j w_j}. \quad (4.5)$$

where the weighting factor w_j is defined as $w_j = 1/(P_j(k) - \bar{P}(k))^2$.

Demonstrating the effect of this weighted averaging, a B-scan taken through a zebrafish head was used. The pigmentation in the eyes of in this case causes specular reflections for a few A-scans within the B-scan. While the averaged background spectra method creates horizontal lines at the depth location of the major specular reflection, the weighted average reduces this effect and improves the image quality.

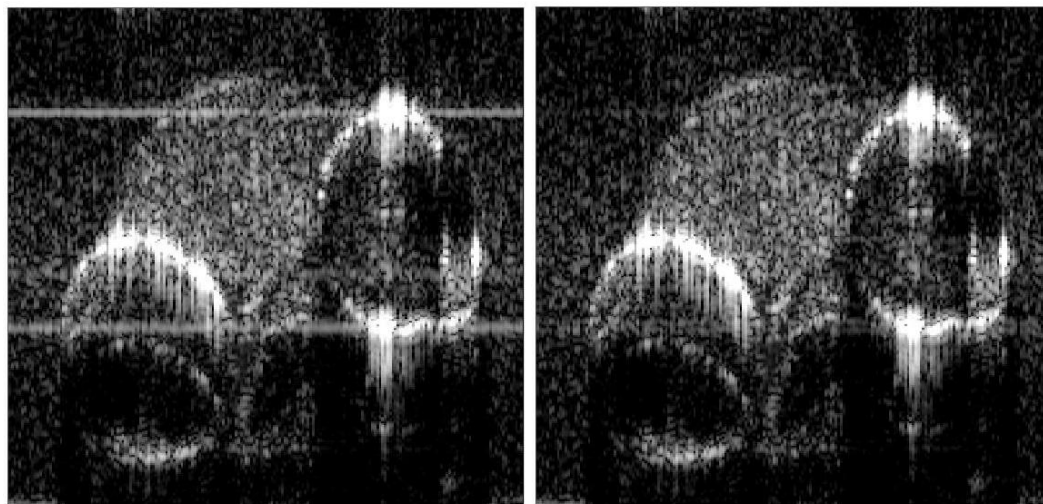


Figure 4.4: B-scans of 3dpf zebrafish head demonstrating specular reflection. The image created using an averaged B-scan as background (left) shows several artifacts. The weighted B-scan as background (right) demonstrates reduced artifacts in this case.

4.3 Sample Preparation

A key aspect in maintaining a stationary sample for in vivo zebrafish imaging is the mounting of the animal. While agarose is excellent for keeping objects stationary within its gelatinous structure, the heat of the liquid form can damage or kill the animal during the mounting process. Regular agarose has a melting point of 88.9 °C to transition from the solid into the liquid form and the gelling point begins at 36.7 °C. To mount the zebrafish, the agarose must remain liquid at a temperature lower than 37 °C to keep the embryo healthy. Low melt agarose is a variation of agarose which has a melting point of 65.1 °C and a gelling point of 26.4 °C, allowing for mounting for in vivo imaging [4]. The zebrafish

to be imaged were anesthetized using a Tricaine solution before being placed in the agarose. A 2% solution of low melt agarose in egg water was used to keep the zebrafish stationary while providing it with the required nutrients supplied by the egg water.

The orientation of the zebrafish while mounting determines the type of images possible with the system. The brightfield confocal image and the GFP labeled vascular image shown in Figures 4.1 and 4.2 both have the zebrafish aligned transversely, with the embryo resting on its side. Unless otherwise stated, the SDOCT images presented for zebrafish imaging were performed with the zebrafish resting on its side such that the major blood vessels along the tail are separated transversely from each other. This alignment also ensures that the majority of the blood flow runs transverse to the imaging direction, demonstrating phase variance motion contrast for the case of severely reduced axial flow components.

When aligning the SDOCT image of the zebrafish, there are several factors to consider for optimizing the image quality:

- Aligning focus of the sample arm is important to maximize the collection efficiency of the sample reflections and determine the transverse resolution. The maximum collection efficiency was aligned to halfway through the depth of the sample.
- Aligning the reference arm should position the interference image within the imaging depth of the SDOCT system. Keeping the sample image near the DC term of the OCT image reduces the SNR penalty that occurs over the imaging depth, but mirror terms and spectrometer noise terms limit the optimal alignment in the image.
- Optimizing the relative polarization between the two interferometer arms improves the SNR of the OCT image.
- Dispersion compensation, spectrometer calibration, and spectral reshaping all have an effect on the OCT image quality.

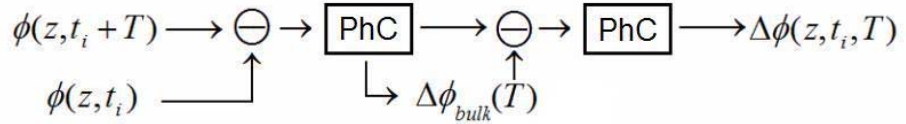
By maintaining a consistent practice of OCT imaging, any variability between phase contrast images can be attributed to sample properties.

4.4 Bulk motion removal

With the large time separations between phase measurements performed with the phase contrast calculations, the system becomes more sensitive to bulk motion between the system and sample. Axial motion of approximately 200 nm within this time will cause an apparent phase motion of the sample reflection of π , obscuring all other motion that can be observed. For $T = 10$ ms, this motion is caused by a bulk velocity of 20 $\mu\text{m/s}$. While minimizing this velocity is possible for the controlled situation observed in microscopy, it will not be the case in general for in vivo retinal imaging situations. It is important to develop methods to deal with the bulk motion experienced and remove it from the phase measurements in the system.

In the phase processing for a given pixel, each phase change calculated for a time separation T is subject to phase conditioning, a term referring in this system to the modulus limitation of phase changes to be within $-\pi$ to π (a phase change of $\pi + \delta$ is conditioned to be $-\pi + \delta$). After the bulk motion calculation of the system motion and the removal from the calculated phase change at a depth z , the resulting corrected phase change undergoes phase conditioning as well. After the second phase conditioning is the phase change used to calculate the variance for the phase contrast images.

For 2 phase measurements separated by time T :



Repeated for N phase changes :

$$\{\Delta\phi(z, t_i, T)\}_{i=1, \dots, N} \longrightarrow \sigma_{\Delta\phi}^2(z, T)$$

Figure 4.5: Data processing schematic for calculating phase variance. PhC: Phase conditioning method which uses a modulus function to limit the calculated phase changes between $-\pi$ and π .

There are several different methods used to determine the bulk axial motion of the sample during the time separation T . Using all of the measured phase changes from all of the

depths in the sample, the mode can calculate the most prevalent phase change within the sample. This method can be very accurate in determining bulk motion, but depends on the depth sampling of the image, as well as the binning parameters for the histogram used to calculate the mode [5].

The main limitation in the bulk phase motion is the SNR-limited phase error, obfuscating the motion calculated for the low signal pixels. While the mean phase change allows for the calculation of the bulk motion, the result can be skewed by the noise terms and the phase conditioning limitation of the range of phase changes. To reduce the effect of the noise terms on the bulk phase change calculation, a weighted mean calculation was used:

$$\Delta\phi_{\text{bulk}}(T) = \frac{\sum_z [I(z)\Delta\phi(z, T)]}{\sum_z [I(z)]}. \quad (4.6)$$

The weighting factor used in the calculations was the OCT signal amplitude $I(z)$, not the magnitude $|I(z)|^2$ as might be expected to remove the noise terms completely from the calculation. If the weighting was chosen based on the OCT signal magnitude, the bulk motion calculation is based too heavily on the assumption that the highest reflections within the sample were stationary, which is not the case for all samples. Using the amplitude $I(z)$ as the weighting factor does not completely remove all of the effect of the noise terms, so a selected depth region within the sample containing a minimal amount of noise terms must be chosen to calculate the bulk motion. An additional option which was not implemented in the experimental data is to add a Boolean function to the weighting factor, removing the effect of all phase changes with OCT intensity below a chosen value.

The limitations imposed on the maximum phase changes causes some miscalculations for the cases where $\Delta\phi_{\text{bulk}}(T) \approx \pi$. The spread of measured phases appears to be near both π and $-\pi$ for this scenario, as shown in Figure 4.6. The weighted mean in this case would appear to have little or no motion occurring during this time period, which causes false phase contrast to be calculated.

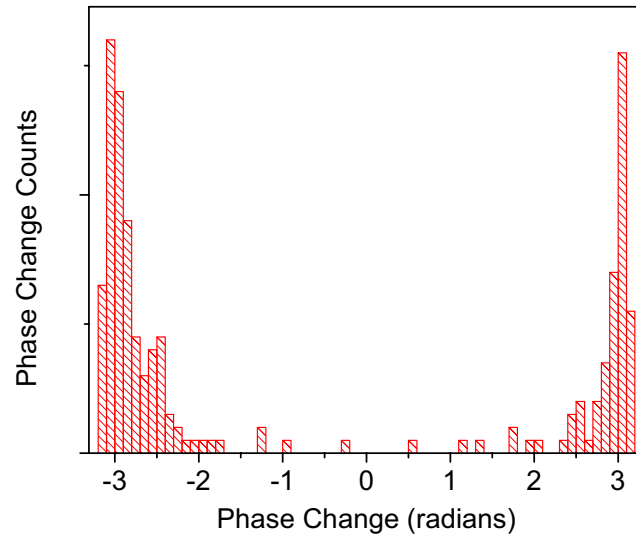


Figure 4.6: Simulated phase change data for bulk motion of $\sim \pi$ radians.

To identify the cases where the bulk motion is $\sim \pi$ radians and additional calculations are required for motion compensation, the phase change data was split up into the cases of $\Delta\phi(z,T) > 0$ and $\Delta\phi(z,T) < 0$. The mean values calculated for these two cases are designated μ_+ and μ_- , respectively. For the case of $\mu_+ > \pi/2$ and $\mu_- < \pi/2$, the phase change range is adjusted to be a 2π phase range centered around $\Delta\phi = (\mu_+ - \mu_-)/2$, and the bulk motion is recalculated properly.

4.5 Zebrafish Tail Contrast Imaging: MB-Scan versus BM-scan

To compare the phase contrast capabilities of the MB-scan and BM-scan methods, both techniques were applied to the same scan region over the tail and yolk sac of a 3 dpf zebrafish. The approximate scan location is depicted graphically on the confocal images of Figure 4.7. By scanning across the zebrafish from the dorsal to the ventral side, the OCT scan is expected to cross two main vessels along the tail, referred to in this case as the dorsal aorta and the axial vein. Through microscopy, estimates of the flow within these tail vessels for 3 dpf zebrafish are approximately 0.5 mm/s.

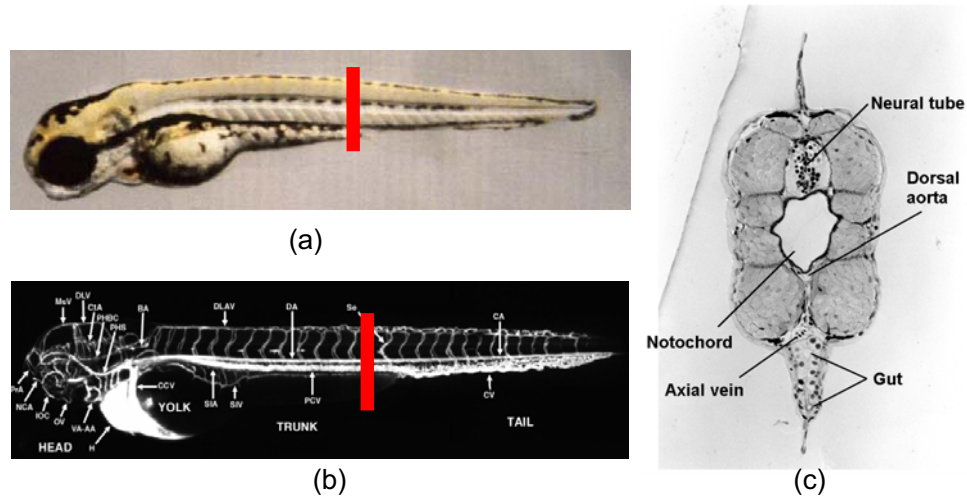


Figure 4.7 a): Confocal bright field image (a) and angiography vascular image (b) containing the approximate transverse scan location for the zebrafish tail phase variance contrast images. The expected histology for the approximate region (c) is also presented.

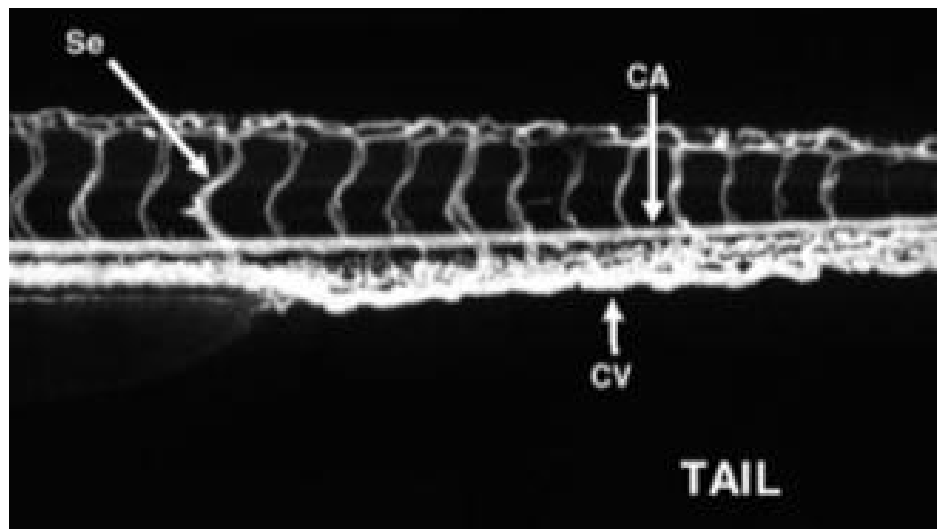


Figure 4.7 b): Zebrafish vascular image from Figure 4.2, zoomed in on tail to highlight the three major vasculature forms: the axial vein/caudal vein (CV), the dorsal aorta/carotid artery (CA) and the segmental vessels (Se).

The MB-scan and the BM-scan performed contrast imaging with 200 transverse pixels across a scan range of 480 μm . The averaged OCT intensity image and the phase variance contrast image are calculated as described in Chapter 3.3 for the case of time separation $T_2=1$ ms. The Doppler flow images plotted in Figure 4.8 are defined as the average phase change between successive A-scans. The total number of phase changes used in the

average calculation for the two images in Figure 4.8 is 5 and 100, respectively. While the maximum phase change scale for these images is $\pm \pi$ radians, both images use a phase scale of ± 0.12 radians which corresponds to an axial flow rate of $200 \mu\text{m/s}$. Using the same scale on both images demonstrates the reduction in phase noise which occurs with increased averaging.

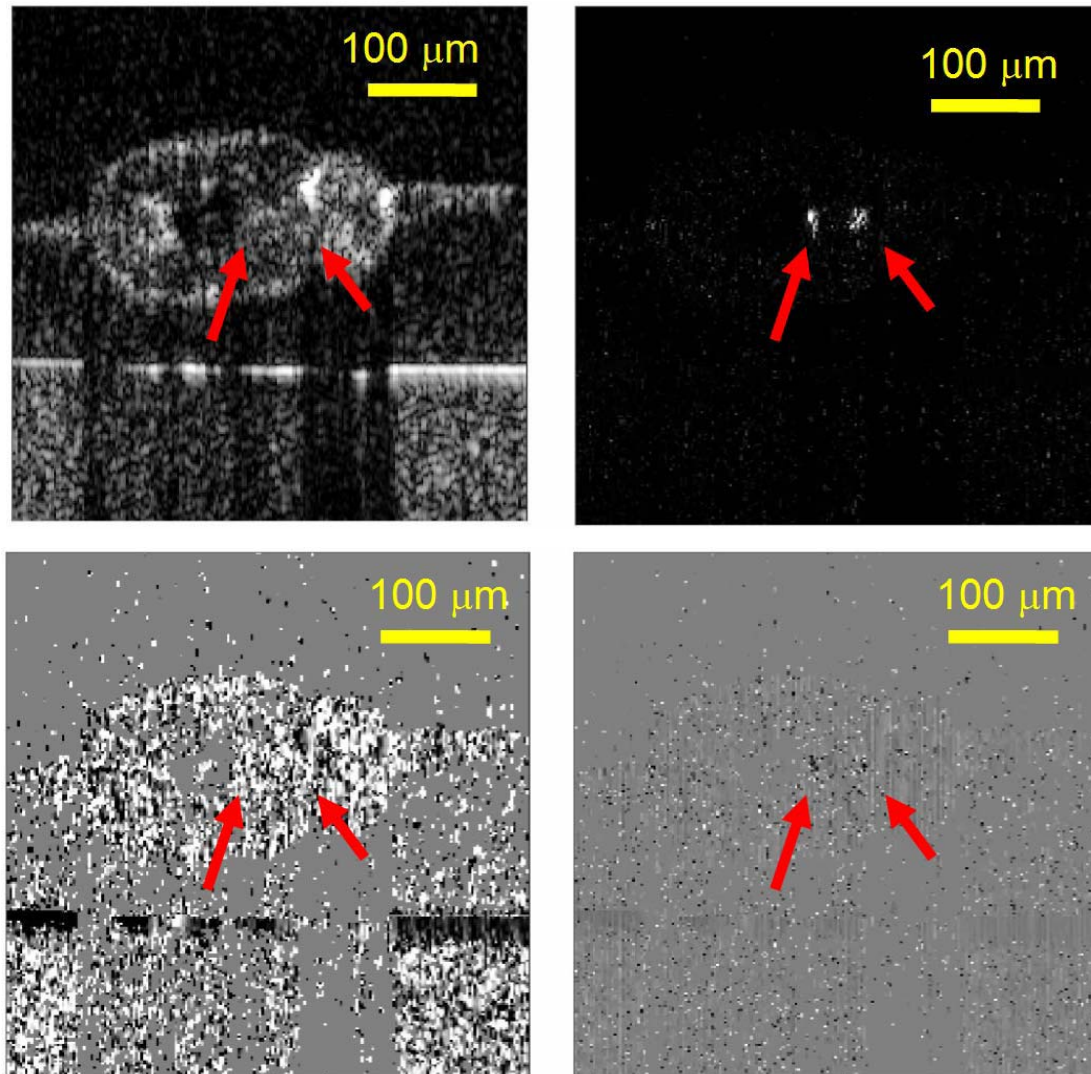


Figure 4.8: MB-scan zebrafish tail motion images with averaged intensity image (upper left). Phase contrast image (upper right) uses $T_2=1 \text{ ms}$ and $T_1= 40 \mu\text{s}$ with a variance scale of 0 to 2 radians². Doppler flow images use scale of ± 0.12 radians = $\pm 200 \mu\text{m/s}$ for the cases of 5 (lower left) and 100 (lower right) phase change averages. Arrows correspond to identified locations of dorsal aorta and axial vein.

The arrows on all four images correspond to the spatial locations of the dorsal aorta and the axial vein. While there is no discernable contrast of the OCT image for these locations, the phase contrast image identifies the motion associated with the flow within the vessels. The Doppler flow image for 5 averages similarly suffers from an inability to observe this flow, evident by the partial visualization which occurs when the averages increase to 100 for this case.

The BM-scan taken over the same region produces the averaged OCT images and phase variance contrast images with an acquisition time of 50 ms. The phase contrast image uses time separations for the phase changes of $T = 10$ ms and applies a rank 1 median filter in each direction of the image. There are no Doppler flow images with this case because the maximum axial flow that can be observed with this method before artifacts occur is 250 times smaller than the previously presented case.

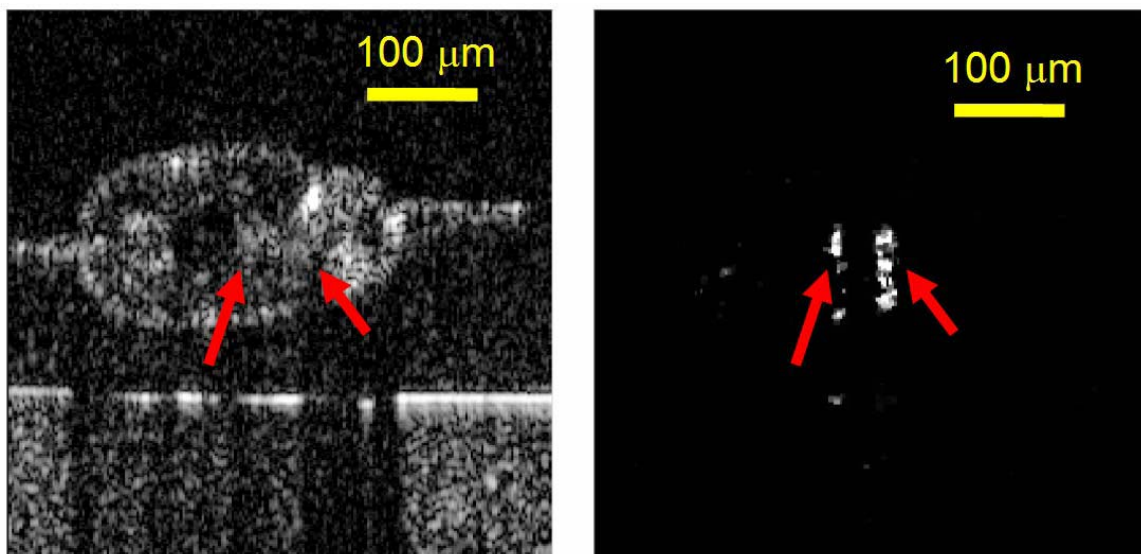


Figure 4.9: BM-scan zebrafish tail images. Averaged OCT intensity image (left) is compared against the phase variance contrast image, using 5 total B-scans, a rank 1 median filter in each direction, and a variance scale of 0 to 3 radians². Arrows correspond to identified locations of dorsal aorta and axial vein.

The major distinction between the phase variance contrast images of the MB-scan and the BM-scan is the visualization which occurs for motion in each method. While both methods observe motion contrast in the regions expected for the dorsal aorta and the axial vein

(designated by arrows), the BM-scan motion contrast also contains a shadowing artifact: motion contrast calculated below the regions of flow where no contrast is expected.

The phase measurement in OCT is not simply a change in the position of a given reflector; it is the change in the optical path length to that same reflector. Therefore, a phase change also measures all of the refractive index variations which have occurred during the time separation T over the entire depth until the measured reflection.

$$\Delta\phi(z, T) = \frac{4\pi}{\lambda_0} \left(\int_0^z \Delta n(z', T) dz' + n(z) \Delta z \right) \quad (4.7)$$

For a stationary reflector measured below a region of refractive index variations (i.e., flow) $\Delta n(z', T)$ which extends a depth of z_n , the calculated phase change is:

$$\Delta\phi(z, T) = \frac{4\pi}{\lambda_0} \Delta\bar{n}(T) z_n. \quad (4.8)$$

To create a completely random phase measurement measured below flow of a vessel of thickness $15 \mu\text{m}$, the required minimum average refractive index variation in this case is:

$$\frac{\Delta\bar{n}_{rms}(T)}{\bar{n}} \approx 0.006 = 0.6\%. \quad (4.9)$$

The observed contrast shadowing is not a complete line through the entire depth of the image due to the numerical SNR phase noise removal performed on the image. The purely noise pixels in the image have no way to differentiate these two types of phase variance, especially when the values are near to the random phase noise limit imposed through the phase conditioning of the data.

To compare the locations of motion contrast to the structural information, the phase variance contrast data over 1 radian^2 was overlapped on the averaged OCT intensity image. This overlap was produced for the MB-scan and the BM-scan to demonstrate consistency to the anatomical structure identified through histology for a similar location within the zebrafish.

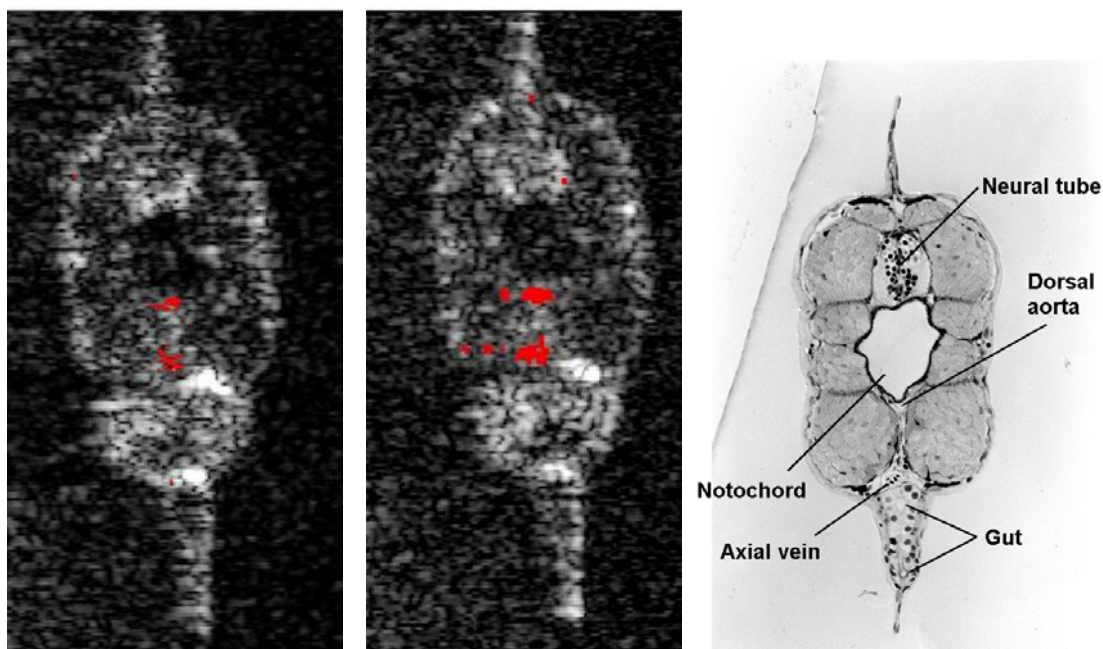


Figure 4.10: Overlay images created from intensity and phase contrast images for the cases of MB-scan (left) and BM-scan (center) compare with histology from similar transverse region of the zebrafish (right).

The MB-scan and BM-scan methods were repeated for a different region of zebrafish tail than used for the images of Figures 4.8 and 4.9, further along the tail past the end of the yolk sac. In this case, the MB-scan phase contrast image can just barely visualize three regions of motion (labeled by arrows) not easily observable in the Doppler flow image. These regions correspond to the dorsal aorta, the axial vein, and the vasculature which connects the segmental vessels on the dorsal side of the zebrafish, referred to as the dorsal longitudinal vessel (DLV). The phase noise image demonstrates, on the same scale as the phase contrast image, the minimum resolvable phase change for the given pixel of the image. The scales on the MB-scan images are identical to the parameters chosen for Figure 4.8.

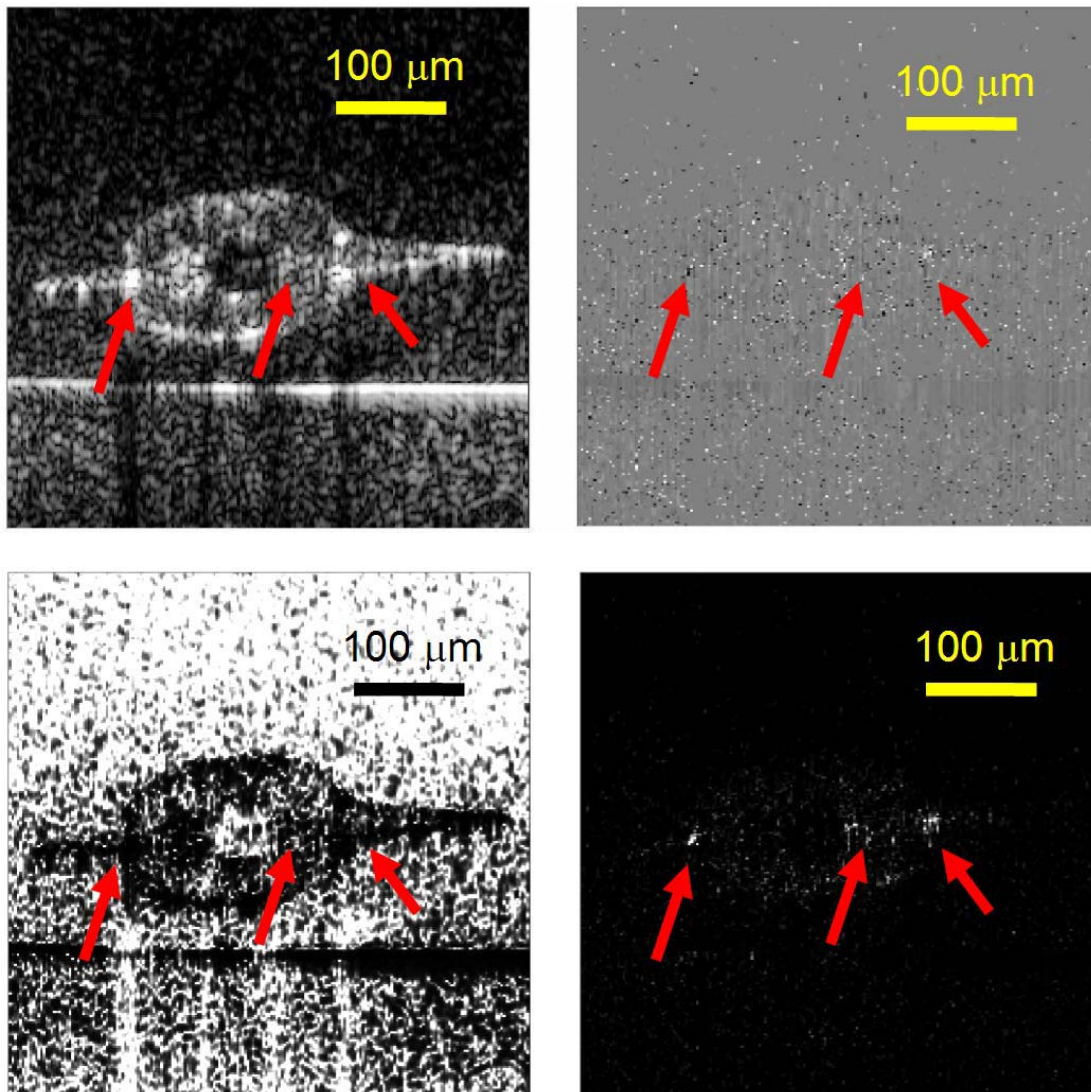


Figure 4.11: MB-scan averaged intensity image (upper left) and phase images for a different region of the zebrafish tail. The phase images include the Doppler flow image for 100 averages (upper right), the measured phase noise in image (lower left), and phase variance contrast (lower right) measured above phase noise. Arrows correspond to identified locations of the dorsal aorta, axial vein, and the dorsal longitudinal vessel.

Repeating the MB-scan over the same scan region, the calculated phase contrast image demonstrates different motion contrast than previously demonstrated. In this case, two of the three expected contrast regions are very hard to identify without prior knowledge of the vascular structure. The BM-scan over the same region does not appear to have any visualization problems observing the motion contrast from the transverse flow in the tail.

Therefore due to improved visualization of BM-scan over MB-scan for the visualization of the zebrafish vascular flow and the improved acquisition efficiency of the method, the BM-scan will be used for all further zebrafish contrast imaging.

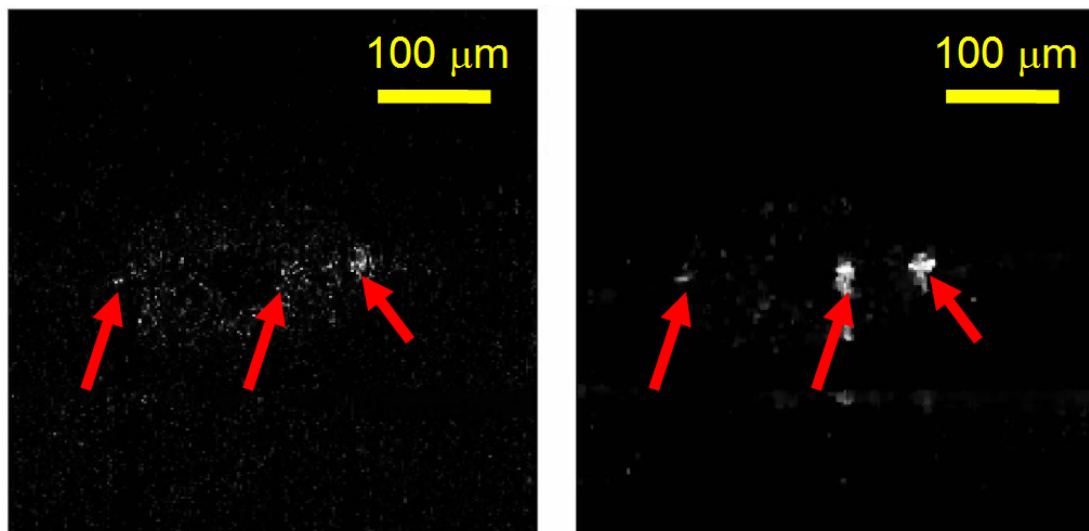


Figure 4.12: Comparing phase contrast images from the two different demonstrated methods for the zebrafish tail location used in Figure 4.11. The MB-scan contrast image (left) is presented with a variance scale of 0 to 2 radians² and the BM-scan (right) uses a scale of 0 to 3 radians². Arrows correspond to identified locations of the dorsal aorta, axial vein, and the dorsal longitudinal vessel.

4.6 Zebrafish Tail Motion Contrast over Time

The phase contrast observed in the zebrafish tail appeared to depend on the time of the image acquisition. Due to the pulsatility observation limitations of the MB-scan, this property could not be studied further using that method. The BM-scan has the ability of looking at the phase contrast image for a given 50 ms time window within a 2.6 s total time acquisition, which allows for the observation of phase variance contrast over time. Looking at multiple phase contrast images over time, five regions of contrast were observed (arrows). While the regions associated with the dorsal aorta and the axial vein maintained visualization over almost the entire acquisition time, the three regions associated with portions of the segmental vessels observed contrast that was almost random in time. Microscopy has confirmed that the blood cells are not flowing through the segmental

vessels for all time points, leading to the assumption that blood flow can be observed within the segmental vessels only when blood is located within the vessel at the acquisition time of the phase contrast image.

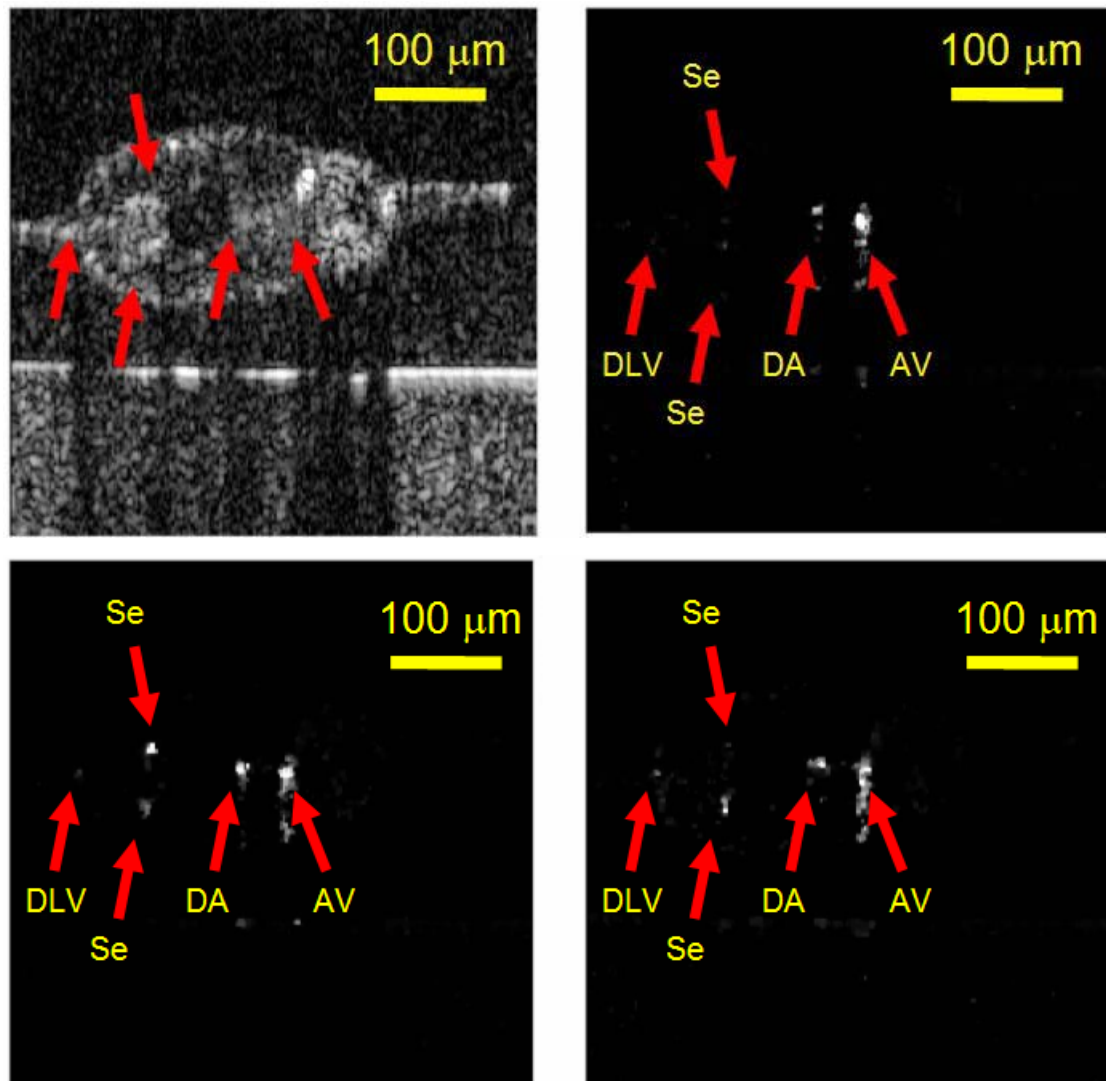


Figure 4.13: BM-scan averaged OCT intensity image (upper left) and three-phase variance contrast images acquired at different time points. Each image was acquired within a total time of 50 ms. The arrows correspond to locations of the dorsal longitudinal vessel, two different segmental vessels (Se), the dorsal aorta (DA), and the axial vein (AV).

To characterize the motion contrast over time for the five contrast regions, a summation image was used to simplify a two-dimensional phase contrast image into a one-dimensional contrast measurement over transverse location. To create a summation image, a depth region of an image is chosen over a portion of the entire depth. The image values for that depth region are summed for each transverse location to create a summation versus transverse pixel calculation. Repeating this method for multiple two-dimensional images of a three-dimensional data set creates an en face, or transverse image from the data set. Creating a summation calculation for multiple images over time allows for the phase contrast to be calculated over time for a given transverse location.

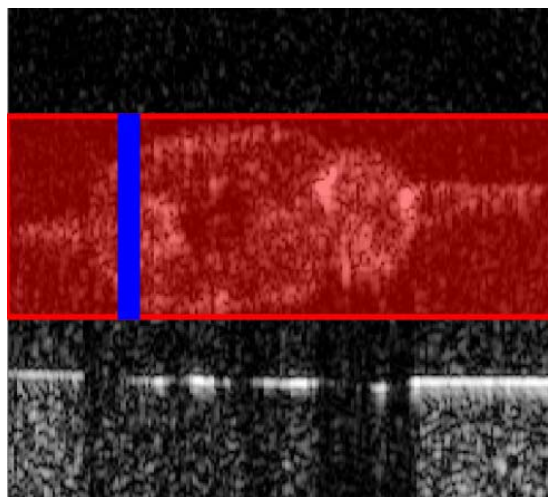


Figure 4.14: Summation images convert each 2D image into a 1D measurement through the depth summation of a chosen region at each transverse location. This method is used to convert a 3D data set into an en face image.

For the phase contrast images calculated for the same B-scan region of the zebrafish tail over time, the contrast was observed for the regions identified by the arrows in Figure 4.13. For each of the contrast summations used in the analysis of this data, the region used for each summation was 3 transverse pixels and 15 axial pixels, corresponding to a region of approximately $7 \mu\text{m} \times 29 \mu\text{m}$. The depth summation region was chosen to be larger than the expected motion contrast region to reduce the alignment errors of choosing the summation regions.

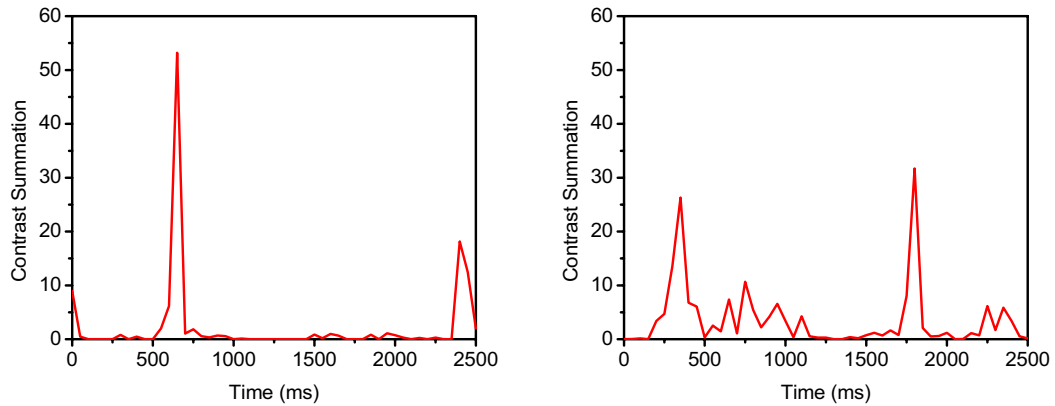


Figure 4.15: Segmental vessel phase variance contrast over time. The segmental vessel closer to top of image (left) was separated from the vessel deeper into sample (right) for contrast analysis. Contrast was summed over 3 transverse pixels and 15 pixels in depth corresponding to $7.2 \mu\text{m}$ in width and $29 \mu\text{m}$ in depth.

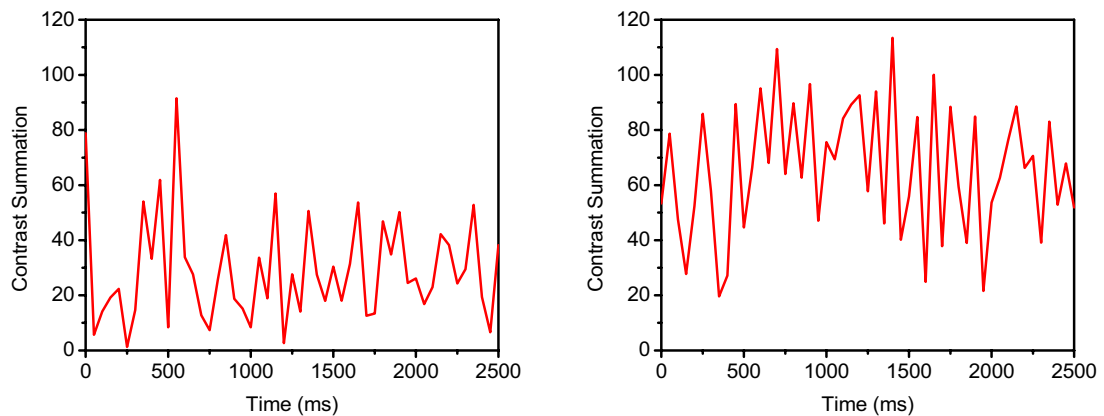


Figure 4.16: Contrast over time of the dorsal aorta (left) and the axial vein (right). Contrast was summed over 3 transverse pixels and 15 pixels in depth corresponding to $7.2 \mu\text{m}$ in width and $29 \mu\text{m}$ in depth.

Looking at the contrast of the segmental vessels over time, it does not match the expected form of contrast from a constant flow within the vessel. Through microscopy, it is observed that the blood cells are not constantly present at all locations within the segmental vessels for a given point in time. This is not an issue for the larger vessels like the dorsal aorta and the axial vein, which both appear to be full of blood cells flowing through them at any given time. This corresponds to the contrast summations taken for the dorsal aorta and the axial vein for the same summation region. While both vessels appear to have motion

contrast for almost all points during the 2.6 s of acquisition time of the phase contrast data, the contrast appears lower in general for the dorsal aorta. By comparing the mean contrast summation of the two cases, the axial vein contrast summation mean is 2.27 times larger than the calculated mean for the dorsal aorta. If we assume that there is identical flow in both of the vessels and the contrast summation captures all of motion of the vessel, this contrast difference would be caused by a vessel diameter of the axial vein approximately 50% larger than the diameter of the dorsal aorta.

Confocal microscopy was used to image the vasculature of a 3 dpf zebrafish, the same age as used in the previously demonstrated phase contrast images. A genetic strain of zebrafish called CT60 was used for imaging in this case. This particular strain of animal has the characteristic of expressing green fluorescent protein (GFP) within its vasculature, allowing for visualization using fluorescent imaging techniques. Using the Zeiss 5 Live laser scanning microscope, the zebrafish vasculature was imaged just posterior to the end of the yolk sac. The zebrafish was oriented on its side for the imaging procedure presented here. Using a high numerical aperture lens, the focal plane within the sample was only a few microns thick. Multiple images were created by focusing the light at different depths within the sample for a fluorescent image. The presented images from that data set are the locations of the dorsal longitudinal vessel and one side of the segmental vessels, the location of the dorsal aorta, and the location of the axial vein and the other segmental vessels.

From these confocal images, many parameters were determined for the 3 dpf zebrafish. The blood flow was approximately 0.5 mm/s for all of the vessels, when the blood cells were moving through them. The segmental vessels and the dorsal longitudinal vessel only contained blood cells within a given location for a fraction of the time. The dorsal aorta and the axial vein, on the other hand, appeared to hold blood cells at all points in time. The heartbeat of the zebrafish affects the pulsatility of the blood flow within the vessels at a rate of approximately 3 Hz.

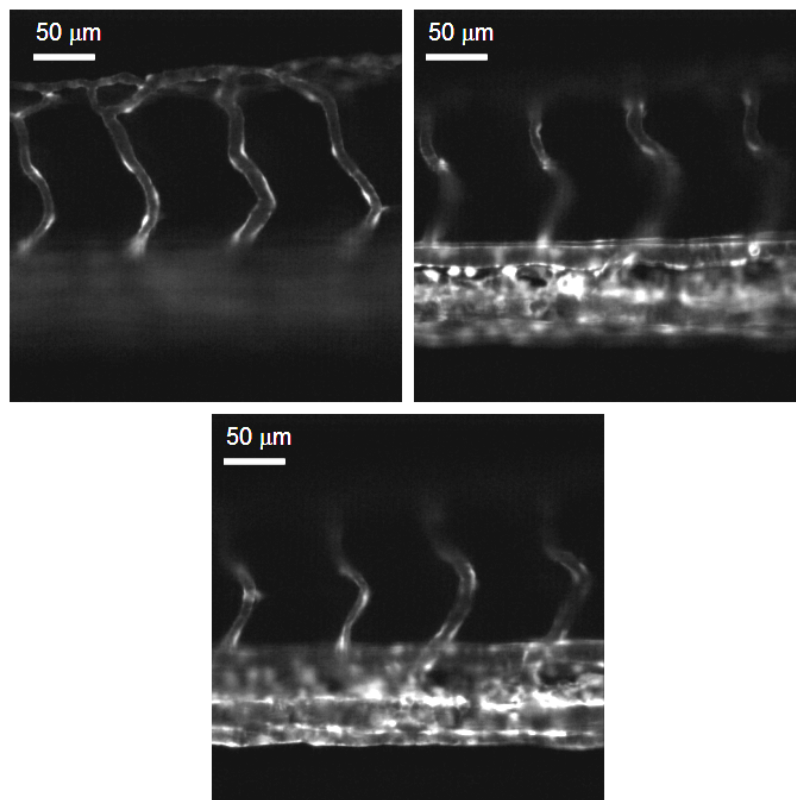


Figure 4.17: High resolution confocal images of GFP-labeled zebrafish vasculature from 3dpf zebrafish genetic strain CT60. Images were produced using Zeiss 5Live confocal microscope. The three images present different focuses within the sample, starting at the shallow segmental vessels and dorsal longitudinal vessel (upper left) and proceeding to focus on the dorsal aorta (upper right), and the deepest focus of the axial vein and the deeper segmental vessels (lower center).

The segmental vessels and the dorsal longitudinal vessel were measured to be 7–12 μm wide, depending on the vessel and the location of the measurement. The measured separation between neighbouring segmental vessels is 75–85 μm for this stage of zebrafish development. The dorsal aorta was measured to have a thickness of approximately 15 μm and the axial vein was the widest in the image with a range of thicknesses from 18–25 μm . The ratio of the range of diameters between the dorsal aorta and the axial vein is 1.2–1.7, consistent with the expected difference determined from the mean contrast summation.

4.7 Segmental Vessel Imaging

Comparing the zebrafish vascular structure to the case of AMD, the segmental vessels which extend from dorsal to ventral sides of the zebrafish might be analogous to choroidal neovascularization (CNV), the main component of wet AMD. In the case of the zebrafish, small vasculature measuring only 7–12 μm wide extends upwards from the blood supply on the ventral side of the zebrafish. This sounds very much like CNV, but in this case the segmental vessels are not leaking into the animal; they are connecting to the dorsal longitudinal vessel and from that to other segmental vessels. By demonstrating the capability of visualizing the segmental vessels using motion contrast, the likelihood of applying these techniques to wet AMD diagnosis is improved dramatically.

To mimic the alignment of CNV within a retinal imaging situation, a different orientation of the zebrafish from the previous images is required. In this case, the zebrafish is positioned with the dorsal side towards the imaging light, allowing the segmental vessels to extend along the depth of the OCT image being created.

The BM-scan parameters used to create the 3D phase contrast image in this case are different than the parameters used in previously presented data. With the small fraction of time in which the blood cells appear to be within a location inside the segmental vessels, the BM-scan acquisition time was increased to try and capture one of these events. The BM-scans used a time separation of $T = 40$ ms for the phase changes, extending over 512 transverse locations. 16 B-scans were used for each BM-scan phase variance contrast calculation and four of these calculations were performed for each transverse scan region by devoting one buffered acquisition of data to each 2D phase contrast image. The mean contrast calculated from the four BM-scans acquired over the same region was used in the 3D phase contrast data set.

By imaging the zebrafish along the dorsal axis for each BM-scan, a minimum number of BM-scans were required to capture all of the 3D data for the embryo. Each B-scan was acquired over a scan length of 650 μm . With an expected segmental vessel separation of

75–85 μm , the 3D zebrafish image over this length should encounter approximately 8 pairs of segmental vessels, increasing the likelihood of visualization. 35 different BM-scan locations were used with 5 μm separation between them, defining the other transverse dimension of the 3D data set as 175 μm .

En face images were created from the OCT averaged intensity 3D data as well as the 3D phase variance contrast data using the summation image method described previously. In this case, each en face image was created through the depth summation of 8 μm around the chosen depth in the data set. The intensity and phase contrast en face images are presented for three different depth locations, corresponding to the upper, middle, and lower bounds of the segmental vessels. The dorsal slice location intercepts the deepest location of the dorsal longitudinal vessel and images the dorsal portion of the segmental vessels. The central slice location is positioned through the notochord of the zebrafish, intercepting all of the segmental vessels along the entire length. The ventral slice location is the dorsal-most slice which encounters the dorsal aorta as well as the deepest portions of the segmental vessels.

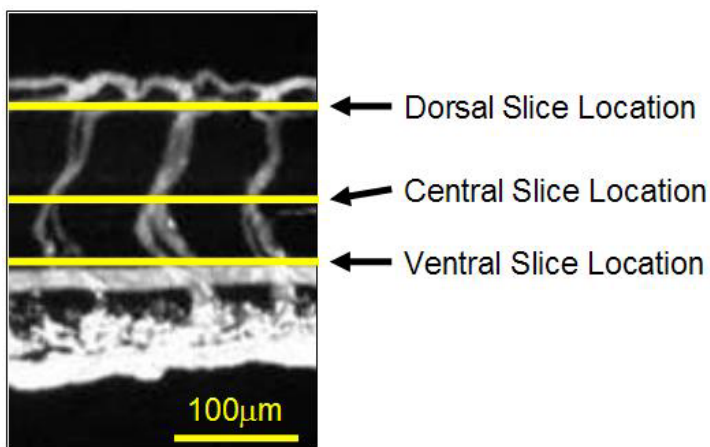


Figure 4.18: Approximate depth locations for the calculated en face slices, presented relative to zoomed in vascular image of Figure 4.2.

The en face intensity images created for the ventral and dorsal slice locations can visualize the main blood vessel due to the increased reflectance from the blood within the vasculature. The central slice, while being able to visualize the structure within the notochord is unable to identify the segmental vessel locations from reflection contrast.

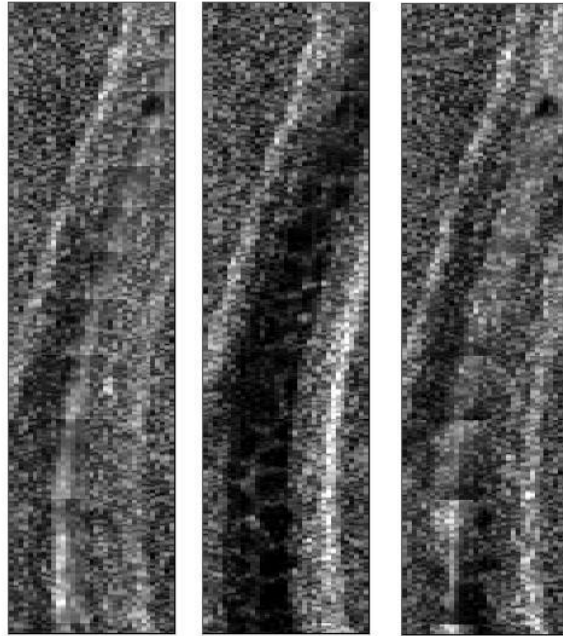


Figure 4.19 a): En face OCT intensity images for the ventral (left), central (middle), and dorsal (right) slice locations designated in Figure 4.18. Image size is $175\ \mu\text{m} \times 650\ \mu\text{m}$.

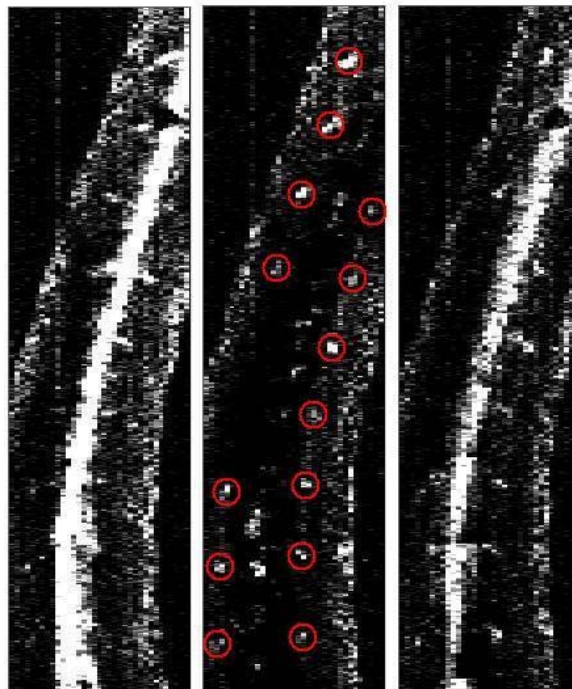


Figure 4.19 b): En face phase contrast images for the ventral (left), central (middle), and dorsal (right) slice locations designated in Figure 4.18. Image size is $175\ \mu\text{m} \times 650\ \mu\text{m}$.

The en face images created from the 3D phase contrast data demonstrate a lot of motion contrast within the zebrafish. The ventral and dorsal slices clearly visualize the transverse flow from the dorsal longitudinal vessel and the dorsal aorta as well as the branching segmental vessels. The central image slice contains many forms of motion contrast, which necessitated the circling of the identified segmental vessels to improve visualization within the image. The motion contrast along the center of the zebrafish in this image is the shadow artifact caused by the flow of the DLV vessel located above it. The contrast observed along the outer edges of the zebrafish is likely due to slight motions of the living embryo over the imaging time. The circled segmental vessels were identified not just from the single slice image, but through the locations of contrast which propagated through multiple depth slices to connect up to the larger vessels above and below. The spacing between the observed segmental vessels in this image is consistent with the expected separation of 75–85 μm along the length of the zebrafish. The two locations on the image which are expected to contain segmental vessel contrast may simply not have any vessels there. Zebrafish do not always create uniform pairs of segmental vessels across their entire length; sometimes there is only one segmental vessel at a position along the length of the embryo. If there are two vessels in the expected locations which do not demonstrate contrast in this data set, the visualization percentage of segmental vessels is 88%.

4.8 En face Images over Zebrafish Heart

Imaging over the zebrafish heart provides a new set of challenges in the data acquisition: the beating heart is moving at a rate faster than the total buffered acquisition of the spectrometer. A data acquisition of phase contrast was acquired while scanning over the beating zebrafish heart. The absorption observed by the light over depth within this region limited the maximum depth which could provide contrast data in this case. The B-scan presented here slices the zebrafish from the dorsal side to the ventral side, with the right portion of the image containing the location of the heart itself. Looking at two different phase contrast images taken through this heart separated spatially by 20 μm along the length of the fish and separated in time by 0.2 s, there is clearly a difference in the observed

size of the heart contrast. Whether this change is due to the spatial or temporal differences of the contrast images cannot be determined from this data set.

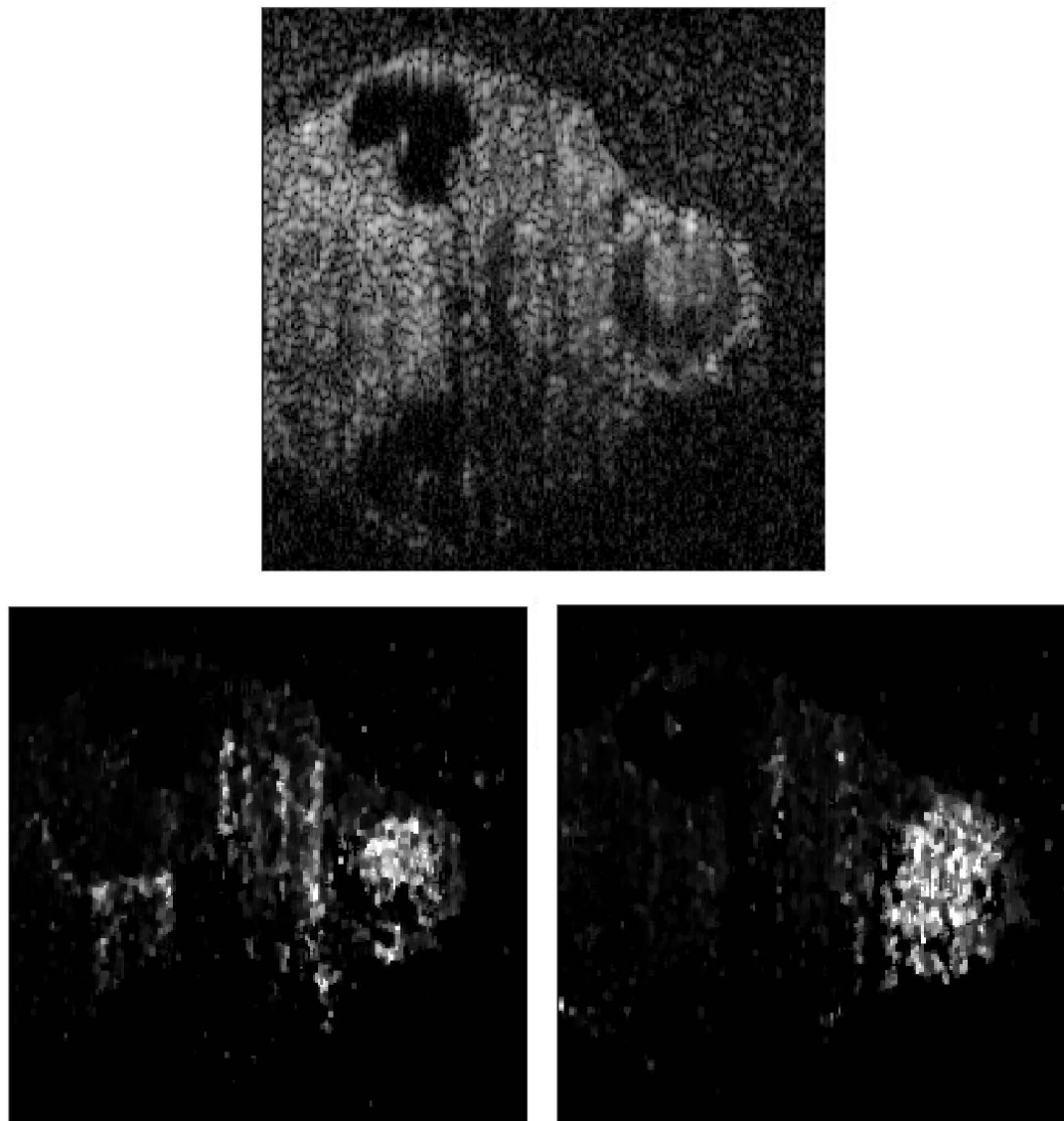


Figure 4.20: BM-scan images over zebrafish heart. The averaged intensity image (upper center) demonstrates the absorption limitation to deep penetration with this light source. The two phase contrast images (lower left and right) were acquired at different transverse slices along the zebrafish separated by $20\ \mu\text{m}$ and 0.2s .

To understand the time scale of the motions with the zebrafish heart, a data acquisition was taken for the same BM-scan location over the heart, acquired over time for 2.6 s. A contrast summation image was created over the entire depth of the image to view the contrast changes associated with the beating heart. While the vasculature near the heart appears to be affected by the beating heart, the contrast never fully disappears within the cycle of the heartbeat. The contrast variations of the heart slice itself can be attributed primarily to the heart physically moving through the chosen slice location during the heart cycle.

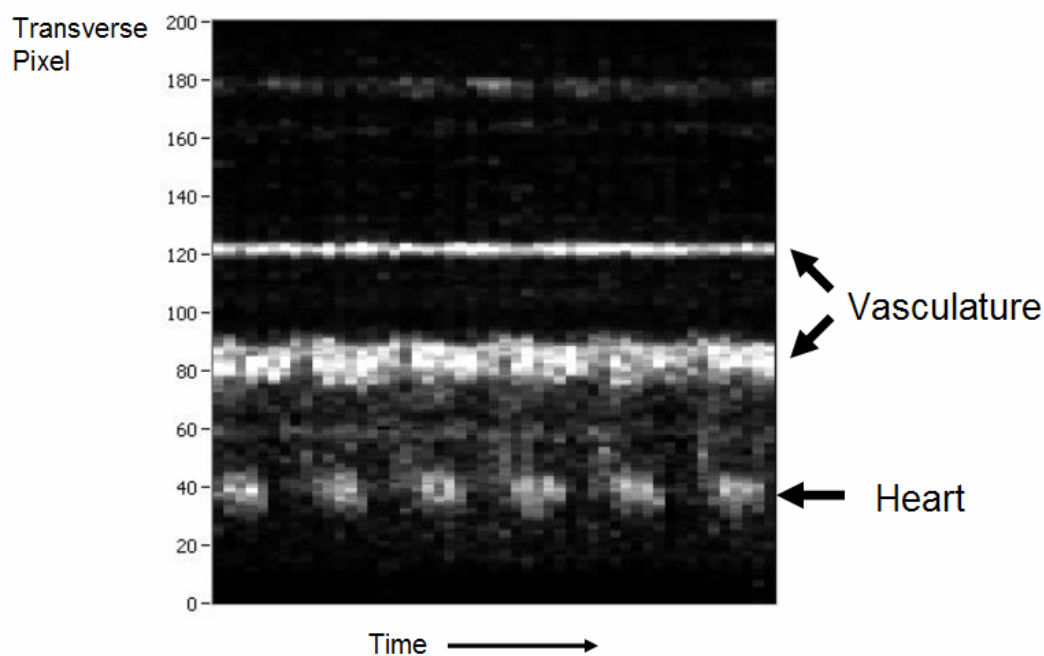


Figure 4.21: Phase contrast summation image over time for a transverse slice located over the zebrafish heart for a total time of 2.6 s. Each time point is acquired in 50 ms.

To analyze the heart contrast over time, the contrast summation was calculated for a region 7 μm wide taken on the heart over the entire depth of the image. The observed contrast in this data appears to have the cyclic nature attributed to the beating heart. From this data, the heartbeat of the imaged zebrafish is estimated to be approximately 2.2 Hz, slower than the expected 3 Hz heart rate determined from confocal microscopy for a similarly aged fish. It is very likely that during the OCT imaging, the zebrafish cooled closer to room temperature from the original temperature of 28 $^{\circ}\text{C}$ of the incubator, slowing the heartbeat.

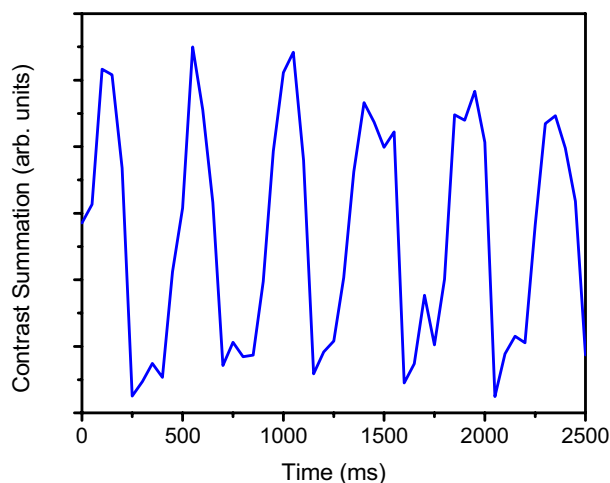


Figure 4.22: Contrast over time for the zebrafish heart at one transverse location. Contrast was summed over 3 transverse pixels ($7.2 \mu\text{m}$) and over the entire depth of the zebrafish.

En face summation images were created from summing over the entire depth of the 3D contrast data taken over the zebrafish heart. No additional data processing was introduced to deal with the beating heart of the zebrafish. Each of the calculated en face images are presented in logarithmic scale to reduce the effect of the contrast fluctuations over time as well as improving visualization of structures within the image itself. To compare against the expected vasculature in the zebrafish, a zoomed in version of the GFP labeled zebrafish confocal image of Figure 4.2 is presented as well. The calculated en face phase variance contrast image is consistent with the vasculature of the 3 dpf zebrafish.

The BM-scan demonstrated the ability to visualize contrast for the range of vasculature, including the segmental vessels, the major arteries of the tail and the heart of the zebrafish. While the zebrafish is a stationary sample in general, heartbeats, digestion, and general motion fluctuations can occur. With the bulk sample motion calculated from the scatterers within the zebrafish as well as the agarose, these motions can affect the bulk removal process. While further progress can be made to improve the analysis procedures, the contrast methods demonstrated show the potential for retinal vascular imaging.

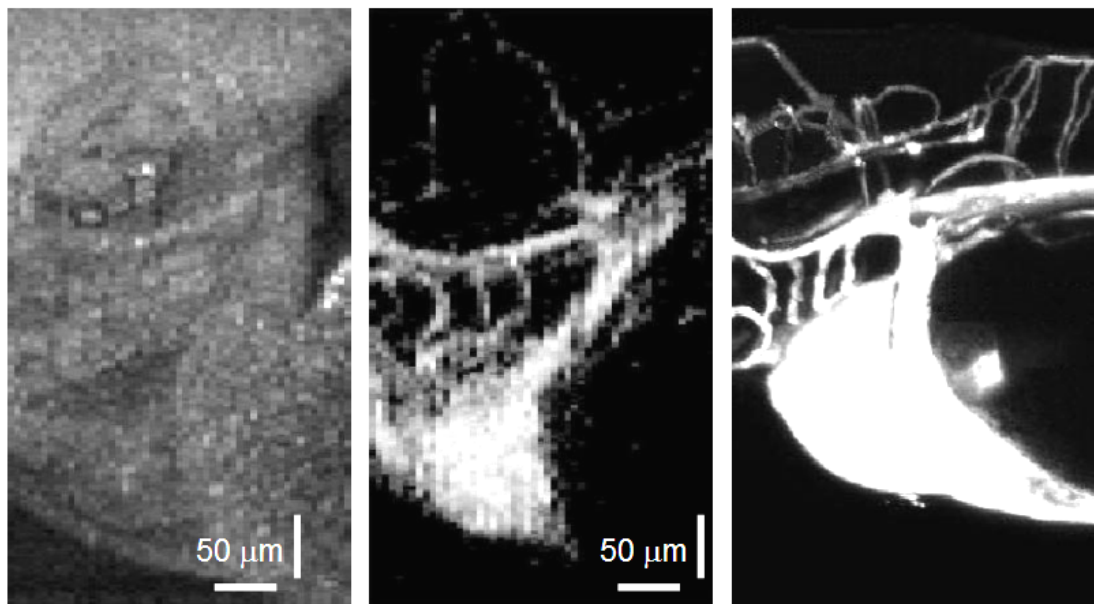


Figure 4.23: En face images over zebrafish heart. OCT intensity summation image was presented in logarithmic scale (left). The phase variance summation image was also presented in logarithmic scale (center) to improve visualization for comparison with a similar region of a confocal image of GFP-labelled 3 dpf zebrafish (right).

4.9 References

1. The Zebrafish Information Network, www.zfin.org .
2. S. Isogai et al., “The vascular anatomy of the developing zebrafish: an atlas of embryonic and early larval development,” *Developmental Biology* 230, 278 (2001).
3. N. Nassif et al., “In vivo human retinal imaging by ultrahigh-speed spectral domain optical coherence tomography,” *Optics Letters* 29, 480 (2004).
4. “Products Catalogue: Agaroses,” Laboratories EUROBIO, http://www.eurobio.fr/UK/secteurs_production/life_science/molecular_biology/Electrophoresis/Products/Agaroses.htm
5. S. Makita et al., “Optical Coherence Angiography,” *Opt. Express* 14, 7821 (2006), <http://www.opticsexpress.org/abstract.cfm?id=97672>.